High-signal-to-noise-ratio laser technique for accurate measurements of spectral line parameters

A. Cygan,[1] D. Lisak,[1] S. Wójtewicz,[1] J. Domysławska,[1] J. T. Hodges,[2] R. S. Trawiński,[1] and R. Ciuryło[1]
[1]*Instytut Fizyki, Uniwersytet Mikołaja Kopernika, ul. Grudziadzka 5/7, 87-100 Toruń, Poland*
[2]*National Institute of Standards and Technology, 100 Bureau Drive, Gaithersburg, Maryland 20899, USA*
(Received 20 September 2011; revised manuscript received 21 December 2011; published 9 February 2012)

An experiment enabling extremely high signal-to-noise ratios in the measurement of spectral line shapes is described. This approach, which combines high-bandwidth locking of a continuous wave probe laser and the frequency-stabilized cavity ring-down spectroscopy technique, enables long-term signal averaging and yields high-resolution spectra with a relatively wide dynamic range and low detection limit. By probing rovibronic transitions of the $^{16}O_2$ B band near $\lambda = 689$ nm, exceptionally precise measurements of absorption line shape and line position are demonstrated. A signal-to-noise ratio of 220 000 and a minimum detectable absorption coefficient of 2.4×10^{-11} cm^{-1} is reported, which corresponds to the lowest line intensity measurable by this setup of approximately 1.3×10^{-30} cm^{-1}/(molecule cm^{-2}). Careful analysis of the data revealed a subtle line-shape asymmetry that could be explained by the speed dependence of the collisional shift. The demonstrated measurement precision enables the quantification of systematic line-shape deviations, which were approximately 1 part in 80 000 of the peak absorption. The influence of slowly drifting etaloning effects on the precision of the line-shape analysis is discussed. How this method can enable experiments that address a number of fundamental physical problems including the accurate optical measurement of the Boltzmann constant and tests of the symmetrization postulate is also discussed.

DOI: 10.1103/PhysRevA.85.022508 PACS number(s): 33.70.−w

I. INTRODUCTION

Recently there have been significant advances in Fourier-transform and laser spectroscopy techniques for measuring absorption line shapes and line parameters. These improvements are associated with increased spectral resolution, higher signal-to-noise ratios (SNRs), and reductions in spectrometer-induced distortions. They enable low-uncertainty measurements of line parameters and increasingly stringent tests of line-shape theories [1–5], the combination of which leads to a better understanding of the physical mechanisms that govern spectral line shapes. For example, the application of advanced line-shape analysis to high-accuracy spectroscopic data [2,4,6] has made it possible to properly quantify and interpret the effects of Dicke narrowing [7] and the speed dependence of collisional broadening and shifting [8] on observed line shapes. High-precision line parameter data required to model low-intensity molecular spectra are important for the next generation of spectroscopic databases [9] to be used in satellite-based remote sensing of the Earth's atmosphere. In a particularly ambitious application, a satellite-borne spectrometer will be deployed to measure column-integrated O_2 and CO_2 concentrations with relative uncertainties <0.5% [10]. Quantitative analysis of the observed spectra will require detailed knowledge of the relevant line-shape parameters with even lower uncertainty, thus motivating the development of high-SNR spectroscopy and validation of line-shape models for these and other atmospherically relevant gas species.

Application of the difference frequency generation (DFG) technique to laser absorption spectroscopy in the near- and mid-infrared regions [11,12] engendered possibilities for precise spectroscopy of molecular line shapes. For decades, DFG laser spectroscopy was a source of high resolution and high-SNR data [13–19] that enabled measurements of several subtle line-shape effects in molecular spectra. The spectrum SNR achieved in these DFG experiments was as high as 10 000 [19]. Also, the development of tunable diode lasers made possible similar measurements in the visible and near-infrared regions [20–25]. In addition to these laser-based approaches, Fourier-transform spectroscopy with broadband incoherent light sources has been widely used for precise line-shape studies of complex molecular spectra [26–28]. A review of various spectroscopic experiments applied to the study of line-shape investigation and associated data analysis methods is presented in Ref. [29]. We note, however, that the experimental methods mentioned above are applicable to relatively strong transitions, whereas similar measurements of weak transitions require long optical path lengths under well-controlled physical conditions. Therefore, cavity-enhanced methods are the most suitable for line-shape studies of weak transitions. The highest previously reported spectrum SNRs were achieved with the frequency-stabilized cavity ring-down spectroscopy method discussed below. These include studies by Long *et al.* [30] (CO_2 lines at 1.6 μm, SNR = 28 000 for a single spectrum), and Long *et al.* [31] (O_2 A-band measurements at 765 nm, SNR = 18 000 for an average of 28 spectra). More recently, De Vizia *et al.* [32] achieved a SNR = 15 000 for a single spectrum of $H_2{}^{18}O$ lines at 1.38 μm, using a cavity-enhanced spectroscopy technique.

There are a number of other important applications of high-performance absorption spectroscopy presented here. The International Committee for Weights and Measures (CIPM) has recommended redefining the fundamental SI unit of temperature (the kelvin) in terms of the Boltzmann constant, k [33]. The most accurate value of k is based upon the acoustic gas thermometry measurements of Moldover [34] and is specified by the Committee on Data for Science and Technology (CODATA) to be $1.3806488(13) \times 10^{-23}$ J K^{-1}. To minimize uncertainty in the new definition of the kelvin, physically independent measurements of k are desired. Among the proposed alternative methods is Doppler-broadening

thermometry of a gas at temperature, T, [35–39] which yields the product kT in terms of the Doppler-broadened width of an isolated absorption line. These experiments require that the line width be measured with a relative uncertainty at the 10^{-6} level. As was shown in Ref. [40] this approach requires extremely high-precision measurements of line shape as well as fitting measured spectra with theory-based profiles that account for collisional broadening, Dicke narrowing, and speed-dependent effects. Several line-shape issues related to optical determination of Boltzmann constant were also discussed in other papers [41,42]. Another fundamental application includes the search for violations of the symmetrization postulate. These experiments rely on extremely high-sensitivity absorption measurements that reduce the upper bound on the strength of forbidden transitions [43–45]. Indeed there are several other cases where high-performance absorption can be used to address fundamental physical questions, such as measuring variations in physical constants [46,47], detection of parity violations in chiral molecules [48], and tests of QED that involve measuring transition rates in atomic spectra [49]. High-performance absorption spectroscopy also allows for detection of isotopic composition [50], deconvolution of hyperfine spectra [51], and may enable the observation of extremely weak ortho-to-para transitions of hydrogen [52].

In this paper we demonstrate extremely high-SNR and high-resolution laser spectroscopy of O_2 B band magnetic dipole transitions [$b\,^1\Sigma_g^+(v=1) \leftarrow X\,^3\Sigma_g^-(v=0)$] near $\lambda =$ 689 nm. This band is commonly used in a number of remote sensing applications, including measurements of cloud-top height and cloud coverage [53,54], stratospheric winds [55], as well as atmospheric pressure and temperature profiles from satellite-borne solar occultation measurements [56]. In the present study, we measured absorption of self-broadened O_2 samples by cavity ring-down spectroscopy.

II. EXPERIMENTAL SETUP

Cavity ring-down spectroscopy (CRDS) is a sensitive laser absorption technique introduced by O'Keefe and Deacon [57] that is based on measuring the absorption-dependent lifetime of photons that exit an optical resonator (ring-down cavity). In the present study, we employ a refinement of CRDS known as frequency-stabilized cavity ring-down spectroscopy (FS-CRDS) [58,59]. A simplified scheme of the FS-CRDS spectrometer [60] is shown in Fig. 1. Technical details of this setup and a thorough description of the measurement procedure can be found in [60,61]. The spectrometer incorporates a mode-matched, rapidly switched, continuous wave external cavity diode laser (ECDL), a length-stabilized two-mirror resonator (<1 MHz cavity mode frequency stability) and a high-bandwidth Pound-Drever-Hall (PDH) lock [62] of the probe laser to the ring-down cavity. Mode-matching ensures single-mode excitation of the resonator TEM_{00} and results in exponential decay signals. The low-bandwidth cavity length stabilization yields a stable and fixed interval spectrum axis necessary for long-term averaging, and the PDH lock maximizes the SNR and the repetition rate (>14 kHz) of the individual ring-down decay signals.

The nominal empty cavity decay time is 9.7 μs based on a mirror reflectivity of 99.975% and a cavity length

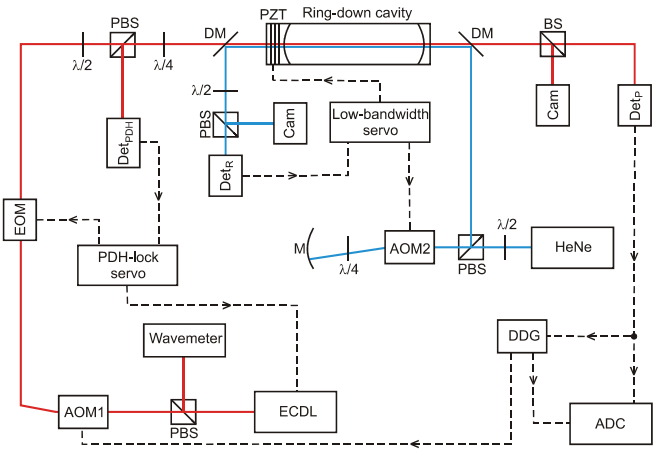

FIG. 1. (Color online) Experimental setup of the PDH-locked FS-CRDS spectrometer. The external-cavity diode laser (ECDL) serves as a probe laser. Its beam is directed into the ring-down cavity and phase modulated by an electro-optic modulator (EOM) to generate the PDH-lock error signal on the PDH detector (Det_{PDH}). The PDH-lock servo controls the probe laser current. The ring-down cavity length is stabilized to the reference HeNe laser by adjusting one ring-down cavity mirror, which is displaced by a piezoelectric transducer (PZT). Cavity length stabilization is achieved with a low-bandwidth FM-lock servo. Here the frequency modulation of the HeNe beam is realized by the acousto-optic modulator (AOM2) and the ring-down cavity transmission signal is measured by the detector (Det_R). Ring-down decays are triggered by a digital delay generator (DDG). When the transmission signal of the probe laser measured by detector (Det_P) reaches a sufficiently high level, the DGG switches off the probe laser beam using acousto-optic modulator (AOM1). At the same time, the DGG triggers data acquisition by the analog-to-digital converter (ADC). PBS is a polarizing beam splitter, DM is a dichroic mirror that separates the HeNe and the probe laser beams, and Cam are the respective cameras used to monitor the transverse modes to which both lasers are locked. $\lambda/2$ and $\lambda/4$ are half and quarter wave plates, respectively, and M is a concave mirror.

of 0.73 m. The free spectral range (FSR) of the cavity is equal to 203.935(2) MHz and corresponds to the frequency interval between consecutive spectrum measurement points presented in this paper. The high-spectral resolution is ensured by active stabilization of the ring-down cavity modes to a frequency-stabilized reference laser [58]. The stability of the frequency axis is of the order of $\pm$1.5 MHz per 3 hours. In the case of perfect mode matching, the PDH technique applied to this system enables the injection of nearly all the laser power into a single cavity mode, with a ring-up and ring-down repetition rate of 14.3 kHz [60]. Typically, 3000 ring-down events are averaged per spectrum point, corresponding to a typical minimum detectable absorption equal to 2×10^{-10} cm^{-1}, as reported in [60]. However, in this article the number of measured decays per spectrum point was set to 1000. This approach allowed us to shorten the measurement time, without considerable degradation of the spectrometer sensitivity. Instead, it was possible to average more spectra in a given time interval. Therefore, the proper detection limit for a single spectrum reported here should be about 3×10^{-10} cm^{-1}.

In our previous article on $^{16}O_2$ B band measurements, we solved the problem of drift in the PDH error signal offset through the use of an active offset control procedure [61]. This approach prevents loss of the PDH lock and is useful for high-repetition-rate cw-CRDS systems in which continuous interruption of the PDH lock leads to instability. The PDH offset correction enables the automatic recording of multiple spectra. The single spectra presented in this paper spanned a frequency range of about 8 GHz (40 measurement points) and were acquired in less than 2.2 minutes. In this paper, acquisition of the highest number of co-added spectra (1040) was realized by alternate back-and-forth frequency tuning of the probe laser and took about 33 hours.

III. LINE-SHAPE MEASUREMENTS AND ANALYSIS

A. Speed-dependent effects on R7 Q8 $^{16}O_2$ transition

The high SNR presented in this work was obtained for the strongest R7 Q8 $^{16}O_2$ B-band line having an intensity of 5.886×10^{-25} cm^{-1}/(molecule cm^{-2}) [63] and measured at a pressure of 933 Pa (7 Torr). This transition was investigated in our earlier papers [64,65]. However, our previously obtained SNR values of 2000 [64] and 6000 [65] were insufficient to distinguish which theoretical line-shape models best described the measured spectra. The following line-shape models: the Galatry profile (GP) [66], the Nelkin-Ghatak profile (NGP) [67,68], the speed-dependent Voigt profile (SDVP) [8], and the speed-dependent Nelkin-Ghatak profile (SDNGP) [67,69], all of which take into account Dicke narrowing [7] and/or the speed dependence of the collisional broadening and shifting [8], gave similar fits to the measured line shape. In this work we used all of these profiles and also the more commonly used Voigt profile (VP). However, as we show below, the SDNGP gives the best fit quality under very high SNR conditions. In the case of the SDVP and SDNGP fits, we used a quadratic model for the speed dependence of the collisional broadening and shifting given by Priem *et al.* [70]. The reduced speed-dependent collisional width and shift functions $B_W(x)$, $B_S(x)$ [71,72] appearing in these line-shape models were approximated by the following functions:

$$B_W(x) = 1 + a_W(x^2 - 3/2), \quad (1)$$

$$B_S(x) = 1 + a_S(x^2 - 3/2), \quad (2)$$

where x denotes the reduced absorber velocity and a_W and a_S are fitted parameters. We note that in our previous investigations of the R7 Q8 $^{16}O_2$ transition, the speed dependence of the collisional shift was ignored because of the small self-shifting value determined for this line [64]. Observation and quantification of this weak effect was precluded by the relatively low value of the spectrum SNR. However, in the present work, the enhanced spectrum SNR that we demonstrated for this transition enabled us to observe asymmetry, which we assign to speed dependence of the collisional shift.

In Figs. 2(a) and 2(b) we present results from SDNGP fits to single and averages of 1040 spectra for the R7 Q8 line, respectively. For the single-spectrum case, the difference in fit quality for the symmetric SDNGP case (without the speed dependence of the collisional shift) and asymmetric SDNGP case (with the speed dependence of the collisional

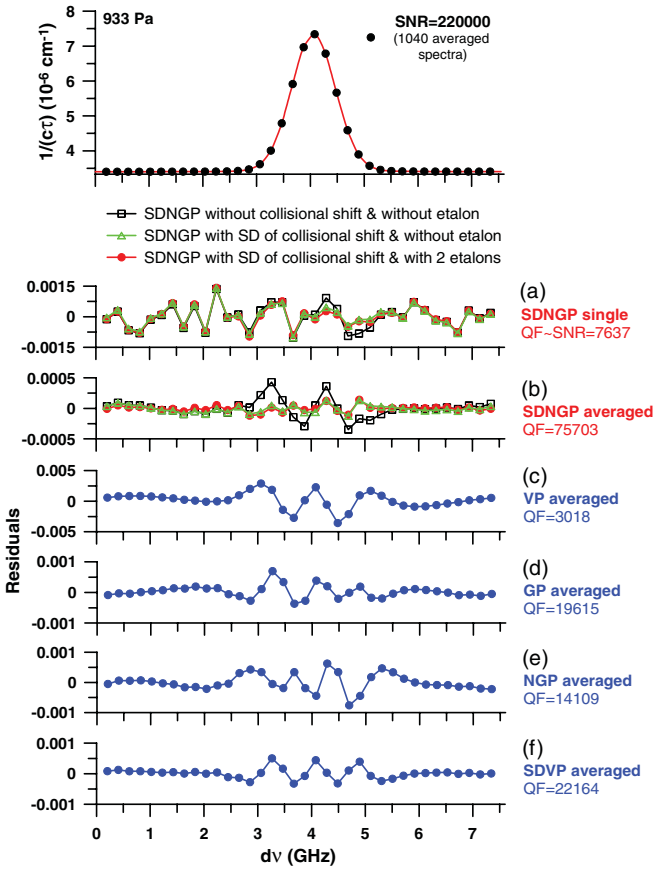

FIG. 2. (Color online) The spectrum of the R7 Q8 $^{16}O_2$ B-band transition measured at pressure 933 Pa. (a), (b) - residuals from SDNGP fits to single and averages of 1040 spectra, respectively. Black squares correspond to SDNGP fits without the speed-dependence of collisional shift and etalons. Green triangles and red dots correspond to SDNGP fits with the speed dependence (SD) of the collisional shift, without and with incorporation of two etalons, respectively. (c)-(f) - residuals from the VP, GP, NGP, SDVP fits taking into account systematic effects caused by two etalons. In the case of the SDVP fit, the speed dependence of the collisional shift was also incorporated. See text for details.

shift) is not readily apparent [compare the black squares and green triangles, respectively in Fig. 2(a)]. On the other hand, for the averaged spectra presented in Fig. 2(b) differences between these two cases are evident. In particular, the residuals presented in Fig. 2(b) corresponding to the SNDGP fit without collisional shifting (black squares) exhibit an asymmetric feature near line center. This asymmetry disappears if the speed dependence of the collisional shift is incorporated into the SDNGP fits [green triangles in Fig. 2(b)]. We note that asymmetry caused by the speed dependence of the collisional shift was observed before for many systems. These include: Ca + Xe [73], Cd + Xe [74], Cd + Kr [75], Ne + Ne [76,77], H_2O + Xe [78], C_2H_2 + Xe [79], H_2O + SF_6 [80], H_2O + N_2 [80,81], and CO_2 + air [82], all of which were measured at a relatively high pressure range. Also, spectrum asymmetry recently was observed for self-colliding $H_2{}^{18}O$ molecules at a pressure of 500 Pa (3.75 Torr) [32]. It should be noted that in the case of the R7 Q8 $^{16}O_2$ line, the expected asymmetry caused by the speed dependence of the collisional shift should

be an order of magnitude smaller than that observed for the $H_2{}^{18}O$ transition measured in Ref. [32]. This is because of the tenfold lower ratio of the collisional shift to the total line width in the case of the $^{16}O_2$ line considered in this study compared to that of the previously investigated $H_2{}^{18}O$ line. For completeness, residuals assuming both the speed dependence of the collisional broadening and shifting as well as etaloning effects (described later) are marked by red points in Figs. 2(a) and 2(b).

Residual plots given in Figs. 2(c)–2(f) correspond to differences between averaged (1040 averages) R7 Q8 line spectra and VP, GP, NGP, and SDVP fits, respectively. For all of these fits, systematic effects associated with two etalons, discussed in the next subsection, also were incorporated. In the case of the SDVP model, both collisional broadening as well as collisional shifting were taken into account. Analysis of residuals from Figs. 2(c)–2(f) shows as expected that the Voigt profile yields the worst results, whereas fit quality is much improved for the GP, NGP, and SDVP cases. We note further that the small asymmetry near line center caused by the speed dependence of the collisional shift (which is apparent for the GP and NGP fits) was removed after application of the SDVP model.

B. Quality of the fit and signal-to-noise ratio

In order to distinguish and quantify the simultaneous effects of systematic distortions and random noise on the measured spectra, we introduce a quantity called the quality of the fit (QF). The QF is defined here as the ratio of the peak absorption signal $\alpha_{\max} - \alpha_{\min}$ to the standard deviation of the fit residuals calculated from the whole spectrum $\widetilde{S}_R$,

$$\mathrm{QF} = (\alpha_{\max} - \alpha_{\min})/\widetilde{S}_R. \tag{3}$$

Here $\alpha_{\max}$ is a sum of the maximum absorption coefficient and the baseline level of the absorption spectrum $\alpha_{\min}$ and $\widetilde{S}_R$ is the standard deviation of fit residuals calculated from the formula

$$\widetilde{S}_R = \sqrt{\frac{1}{M-k}\sum_{i=1}^{M}[\alpha_{\exp}(\nu_i) - \alpha_{\mathrm{fit}}(\nu_i)]^2}, \tag{4}$$

where M is the number of measurement points in a single spectrum, and k is the number of degrees of freedom corresponding to the number of line-shape parameters for a given theoretical model. The terms $\alpha_{\exp}(\nu_i)$ and $\alpha_{\mathrm{fit}}(\nu_i)$ are experimental and fitted absorption coefficients, respectively for a given measurement point of the spectrum.

Similarly, we define the signal-to-noise ratio (SNR) as the ratio of peak absorption signal $\alpha_{\max} - \alpha_{\min}$ to the standard deviation of the fit residuals S_R determined from the portion of the measured spectrum that excludes the 2.5 GHz wide spectral region around the line center. This definition allows us to exclude the influence of the fitted line-shape model on the SNR $= (\alpha_{\max} - \alpha_{\min})/S_R$. For the case of uniform residuals around zero, S_R is a good approximation to the standard deviation of the measured absorption coefficient.

We should emphasize that our definition of QF takes into account not only random noise in the experimental spectrum, as in the case of SNR, but also systematic distortions of the line shape, which for example may be caused by etaloning

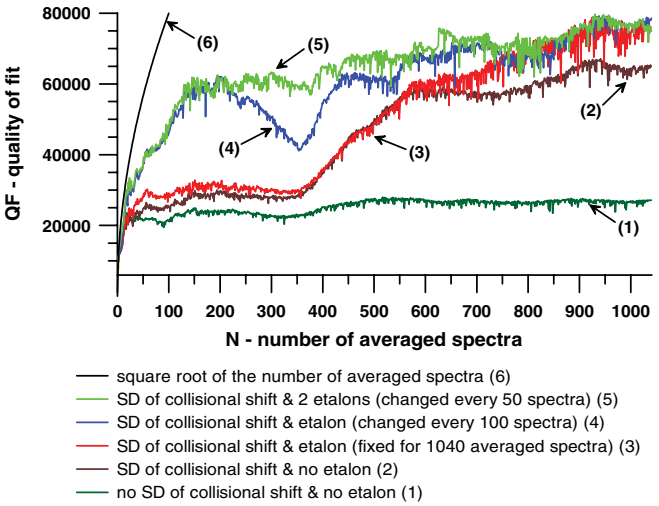

FIG. 3. (Color online) The dependence of the QF value on the number of averaged spectra for the R7 Q8 line in the case of SDNGP fits. (1) No collisional shift and etalons were incorporated into the line analysis. (2)–(5) The speed dependence (SD) of the collisional shift was taken into account in SDNGP fits without etaloning effects in (2), with one etalon fixed for an average of 1040 spectra in (3), with one etalon variable every 100 spectra in (4), with two etalons variable every 50 spectra in (5). (6) The square root of the number of averaged spectra.

effects or limitations in the line-shape model. Therefore, in general, the value of QF can depend on the frequency range in which the spectrum was fitted. Nevertheless, in the case of line-shape models that give perfect fits, both figures-of-merit (i.e., QF and SNR) should give similar results and be should be independent of the frequency range.

In Fig. 3, we summarize the influence of systematic time-varying etalons on the measured QF value for the R7 Q8 O_2 line. All graphs (1)–(5) in Fig. 3 present QF as a function of the number of averaged spectra, N. The calculated QF values for the various line-shape models discussed above are indicated in Fig. 2.

C. Etaloning effects in spectra averaging

One considerable benefit of co-adding spectra is the reduction of periodic and temporally uncorrelated residual features known as etaloning effects [31]. Kassi *et al.* reported long-term averaging (43 spectra acquired over one night) for CRDS measurements of the $a\,^1\Delta_g(v=0) \leftarrow X\,^3\Sigma_g^-(v=0)$ band of O_2 [83]. They found that the spectrum noise decayed faster than the ergodic $1/\sqrt{N}$ dependence. This behavior was ascribed primarily to etalon phase variation caused by thermomechanical system drift occurring over the duration of the measurement, which resulted in rapid reduction of the interference fringe amplitude.

We investigated how the inclusion of speed-dependent collisional shift, number of etalons, and etalon drift influences the evolution of QF with N. These results are summarized in plots (1)–(5) of Fig. 3 for the case of SDNGP fits to the R7 Q8 $^{16}O_2$ B-band line. Of these cases, all but plot (1) of Fig. 3 included the collisional shift effect. For all calculations, the initial line-shape parameters used in the fitting procedure

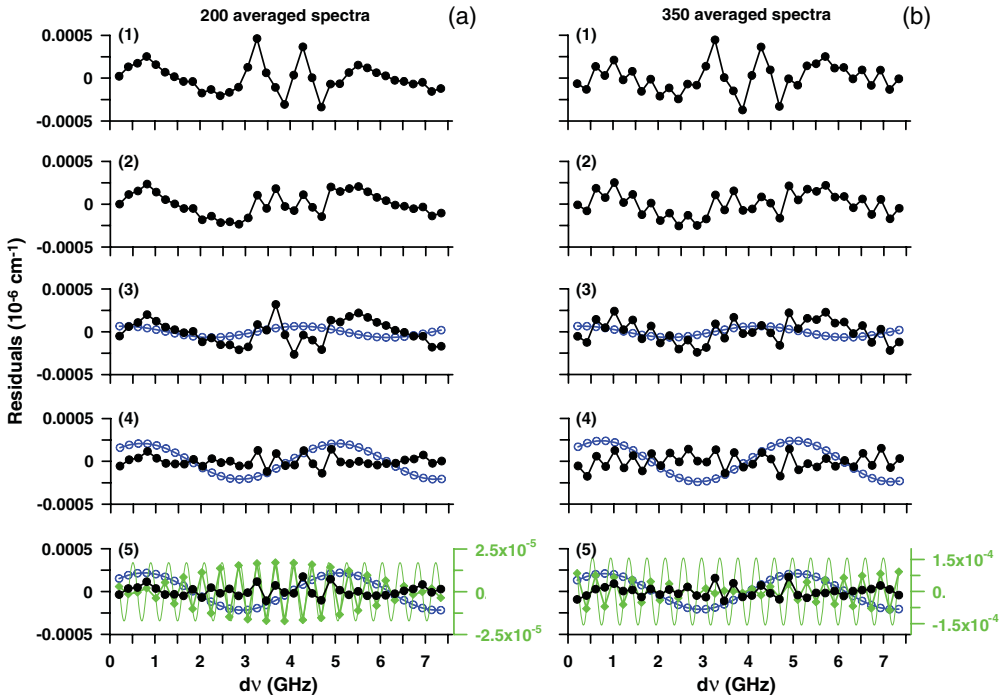

FIG. 4. (Color online) The influence of etaloning effects on the QF value in the case of SDNGP fits for averages of 200 (a) and 350 (b) spectra for the R7 Q8 O_2 transition. Residuals presented in graphs (1)–(5) correspond to the same fitting conditions as those used in the analysis of graphs (1)–(5) of Fig. 3. Blue circles and green diamonds (also green lines) indicate the two etalons taken into account in the line-shape analysis. Differences in etalon shapes between the green line and green diamond plots (green ordinate axis) in graphs (5) result from undersampling density in the latter case.

were the same as the fitted values corresponding to: $N = 1040$, with speed-dependent collisional shift and two etalons. With no etalon or speed-dependent collisional shift [Fig. 3, plot (1)], we find that the QF rapidly increases to a constant value of about 25 000 after averaging only 25 spectra. Figure 3, plot (2) illustrates that incorporation of the speed-dependent shifting effect increases the maximum QF value by about 2.5 times, consistent with the SDNGP residuals shown in Fig. 2(b) (black squares and green triangles). Adding one etalon with a period of about 4.5 GHz to the Fig. 3, plot (2) case results in plot (3), for which the QF(N) dependence is similar in shape to that of plot (2) up to $N = 600$. For larger N, small differences (caused by etaloning effects) between plots (2) and (3) can be observed. For plot (3), the best etalon parameters were found from SDNGP fits to the average of all spectra, and these etalon parameters were held constant for all the fits used to determine QF(N). In order to account for drift in etalon phase and amplitude, these two parameters were changed every 100 spectra to values that gave the best fit quality, and this result is presented in plot (4) of Fig. 3. We also considered the inclusion of a second etalon (period of about 0.4 GHz), and these results are given in plot (5) of Fig. 3. Because of the higher frequency of the second etalon, the amplitude and phase of both etalons were changed every 50 spectra in plot (5). We find that plots (4) and (5) for QF(N) are similar throughout the range of N except for the interval $N = 200$ to 700 where the two curves differ appreciably. The largest discrepancy occurs at $N = 350$ and was caused by the second etalon, which was observed in the spectrum baseline. For plot (5), the maximum QF occurred at $N = 947$ and was about 80 000.

To better understand the influence of etaloning effects on the QF value, residuals for two averaged spectra given by $N = 200$ and 350 [panels (a) and (b), respectively of Fig. 4] were calculated for all the cases presented in plots (1)–(5) of Fig. 3. For both values of N, incorporation of the speed dependence of the collisional shift in the SDNGP line-shape analysis improves the fit quality only near the line center [compare graphs (1) and (2) of panels (a) and (b), respectively]. In Fig. 3 this effect is manifest as a small difference in QF(N) of about 6000 between plots (1) and (2). In Fig. 4, graphs (3a) and (3b), we present the fit residuals after taking into account one etalon (denoted by the blue circles). In these cases we also do not see a significant improvement in fit quality compared to graphs (2a) and (2b) [compare also plots (2) and (3) of Fig. 3]. As it turned out, the etalon amplitude and especially phase, determined from the fit of $N = 1040$ averaged spectra, were inadequate for SDNGP fits to $N = 200$ and $N = 350$ averaged spectra. Indeed, for Fig. 4 if one compares the etalon phases from graphs (3a) and (3b) with those seen on the residuals, graphs (2a) and (2b), one can see considerable differences between them. This was the motivation for changing the etalon amplitude and phase every 100 spectra as discussed above. The optimal etalons corresponding to the $N = 200$ and $N = 350$ cases are presented in graphs (4a) and (4b) of Fig. 4, respectively. In these, the shape of the fitted etalon function better reflects the shape of the residuals seen in graphs (2a) and (2b) of Fig. 4. However, the difference between QF values for $N = 200$ and $N = 350$ [see graph (4) in Fig. 3] is about 20 000. This results from the second etalon, which remains uncompensated, and which is most clearly seen for

the case of $N = 350$ averaged spectra [see graphs (1)–(4) in Fig. 4(b)]. Nevertheless, this etalon is present over the entire range between $N = 201$ to $N = 700$ [see plot (4) in Fig. 3]. Considerable improvement in fit quality was obtained after incorporation of the second etalon to the line-shape analysis, as can be seen in the residuals given in graphs (5a) and (5b) of Fig. 4. Under these conditions, the QF values obtained for both values of N considered are similar [compare plot (5) in Fig. 3 and graphs (5a) and (5b) of Fig. 4]. The second etalon presented in Fig. 4 graphs (5a) and (5b) was marked by solid green and green diamond plots. In these graphs, note that the green diamond plot differs from the solid green plot because of undersampling effects.

We note that even the best QF(N) dependence obtained for the R7 Q8 $^{16}O_2$ line [plot (5) in Fig. 3] differs significantly from the $8000\sqrt{N}$ dependence [plot (6) of Fig. 3], expected when the QF is random noise limited. This departure from the random noise limit is caused by additional systematic errors that were not considered in the line-shape analysis and for which detection and assignment is difficult. On the basis of plots (5) and (6) of Fig. 3, one may say that noise-induced statistical effects dominate over systematic effects only in the range $N = 1$ to 20, whereas for longer averaging times the influence of drifting systematic effects on the QF becomes more noticeable. To more carefully analyze the contribution of random noise and its reduction with averaging, we computed the dependence of the standard deviation of the fit residuals $\widetilde{S}_R$, on the number of averaged spectra for the R7 Q8 and R41 R41 $^{16}O_2$ B-band lines, and these results are presented in Fig. 5. Here, the black dashed line and the red solid line correspond to the power-law functions $aN^{-0.5}$ and $a_{\text{fit}}N^{-\mu}$ respectively, where a is the noise amplitude of the first spectrum, a_{fit} is a fitted noise amplitude, and μ is the decay exponent, which was treated as a fitted parameter. In the case of the R7 Q8 transition, a, a_{fit} and μ are: $0.00052 \times 10^{-6}\,\text{cm}^{-1}, 0.00053 \times 10^{-6}\,\text{cm}^{-1}$, and 0.45, respectively. However, we note that the power-law fit for the R7 Q8 line was realized in the range between $N = 1$ and $N = 20$. As seen in Fig. 5, the observed behavior is accurately modeled by a $\widetilde{S}_R(N = 1)/\sqrt{N}$ dependence. This result is consistent with our previous discussion of Fig. 3. As we checked, power fit realizations in the range wider than $N = 1$-20 gave systematically smaller values of μ down to a minimum value of 0.24 corresponding to the case where the data were fit over the entire range of N.

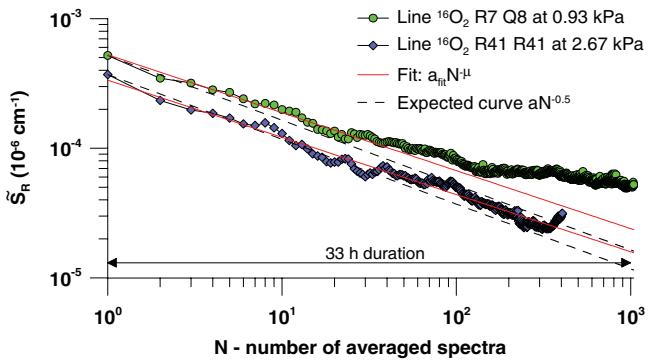

FIG. 5. (Color online) The dependence of $\widetilde{S}_R$ on the number of averaged spectra for R7 Q8 (green dots) and R41 R41 (blue diamonds) O_2 transitions. Red lines are power fits, respectively, to both transitions. In the case of the R7 Q8 line power fit was realized in the range of 1–20 whereas for the R41 R41 line fit covered full data range. Black dashed lines correspond to the $\widetilde{S}_R(N = 1)/\sqrt{N}$ dependence.

D. Influence of systematic errors on precision of line-shape parameters

In our line-shape analysis, we constrained a_S to be equal to a_W and we fit the collisional shift. This was necessary because the collisional shift for the R7 Q8 transition is highly uncertain and is strongly correlated with the a_S parameter. The resulting values of the R7 Q8 line area, the collisional width and shift, the line narrowing, and a_W parameters obtained for the SDNGP are summarized in Table I. These results take into account speed dependence of collisional broadening and collisional shifting as well as etaloning effects.

For all line profile calculations, we fixed the Doppler broadening parameter to the value corresponding to the measured temperature of 295.5(1) K. We note that when the SDNGP is used for data analysis, the asymmetry of the measured line shape can be described by the product of Δa_S of collisional shift Δ and an empirical parameter describing its speed dependence a_S. Assuming equality between the a_W and a_S parameters, we obtained $\Delta = -1.244(33)$ MHz from the fit. Obviously, any change in the assumed value of a_S will lead to a different determination of Δ. Therefore, the parameter Δ should not be assigned to the physical collisional shift. Moreover, the observed line asymmetry can also be caused by several other physical effects, such as correlations between velocity- and phase-changing collisions [14,67,84], finite collision duration time [85], or line mixing [86] (see also Refs. [2,87]).

In Table I we give only statistical uncertainties of the fitted line parameters, consistent with the random noise-limited SNR of our measured spectra. In order to investigate the influence of systematic drifts in precision of the measured line-shape parameters, we computed the Allan deviations [88] of the fitted line center, collisional width, and line area. The black dotted and red circle plots in Fig. 6 correspond to two SDNGP fits, without the speed dependence of the collisional shift and etalons, and with collisional shift and incorporation of two etaloning effects, respectively. For all three fitted parameters, the two Allan deviation curves associated with both fits are quite similar. The blue data shown on each graph represent the time dependence of the given line-shape parameter. As seen from Figs. 6(a)–6(c) any systematic drifts of temperature, pressure, or spectrum frequency axis can seriously limit the optimal number of averaged spectra. In the case of the line area [Fig. 6(c)], satisfactory precision can be obtained after averaging as few as 30 spectra. In the case of the collisional width parameter [Fig. 6(b)], the situation is more complicated because of specific irregularities observed for the Allan deviation function. For this case, more data should be acquired in order to capture the strange behavior of the Allan deviation at the end of the record. For the line center results given in Fig. 6(a), the precision continuously increases with the number of averaged spectra up to $N = 200$. In this case, more spectra should be averaged in order to find the optimal value of N.

TABLE I. Values of the line area A (kHz cm^{-1}), the collisional width (FWHM) γ (MHz), the line narrowing $\nu_{\rm opt}$ (MHz), and the speed-dependence parameter a_W obtained for three oxygen B-band lines measured in this study. Uncertainties of line parameters represent only statistical standard deviations. Temperature T and pressure p in our measurements are given in units of K and kPa, respectively.

Line	Profile	T	p	A	γ	$\nu_{\rm opt}$	a_W
R7 Q8 $^{16}O_2$	SDNGP	295.5(1)	0.9333(5)	4.07420(12)	26.546(41)	0.812(23)	0.0799(11)
R7 Q8 $^{16}O^{17}O$	GP	295.0(1)	26.664(14)	0.04634(24)	0.883(8)	0.0997(54)	–
R41 R41 $^{16}O_2$	GP	295.0(1)	26.664(14)	0.005986(33)	0.4303(55)	0.1312(24)	–

The initial slope of an Allan deviation plot (on a log-log scale) is close to $-1/2$ when the distribution of measured values is approximately Gaussian (see, for example, Ref. [60]). Indeed, we find that the respective Allan deviation curves for the line area and collisional width parameters [Figs. 6(b) and 6(c)] have an initial slope that is nearly equal to $-1/2$. Further, we note that the histogram of measured line areas is essentially Gaussian as evidenced by the fitted distribution shown in Fig. 7(a). We also observed a nearly Gaussian distribution for the measured collisional widths. In contrast, for the fitted line center, the Allan deviation curve exhibits corrugations and its initial slope is not close to $-1/2$ [see Fig. 6(a)]. Also, the histogram of measured line centers exhibits a bimodal, non-Gaussian saddle shape. It should be noted that the nominal 1.1 MHz line center fluctuations seen in Fig. 7(b) are associated with fluctuations in the HeNe reference laser frequency to which our ring-down cavity length and frequency axis are actively stabilized. [58,60,89].

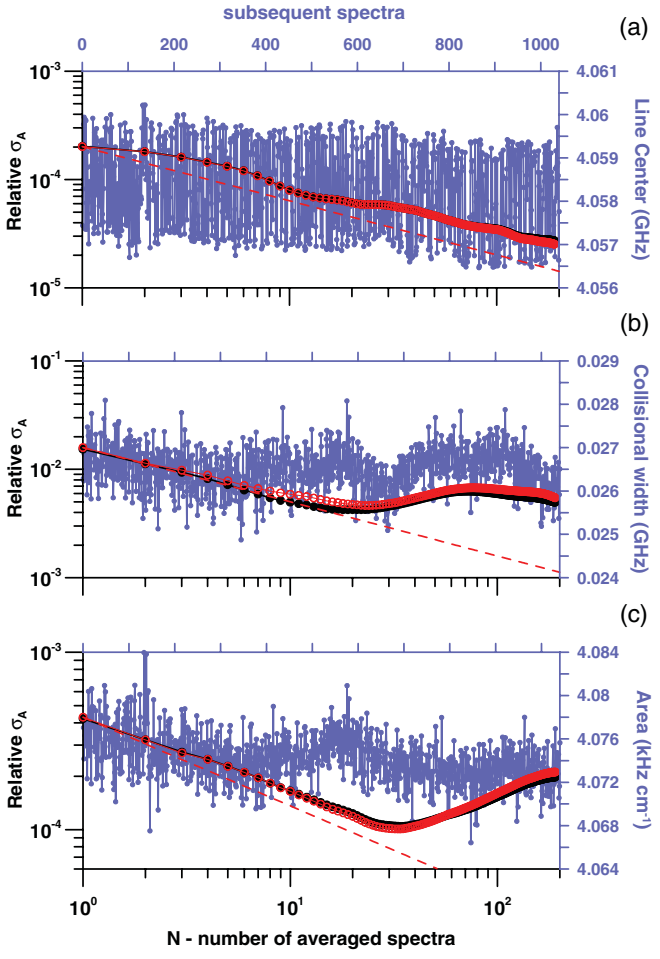

FIG. 6. (Color online) The influence of systematic errors on parameters of the line center (a), the collisional width (b), and the line area (c). The Allan deviation corresponding to SDNGP fits without the speed dependence of collisional shift and etalons was marked by black dots (black axes). The Allan deviation corresponding to SDNGP fits with speed dependence of collisional shift and incorporation of two etaloning effects was marked by red circles (black axes). In this case red dashed lines correspond to the $\sigma_A(N=1)/\sqrt{N}$ dependence. Blue graphs show time dependence (in units of quantity of measured spectra) of the line center, the collisional width, and the line area, respectively (blue axes).

IV. DETECTION LIMIT

To quantify the detection limit, we probed the relatively weak R41 R41 $^{16}O_2$ B-band transition, which has an intensity at room temperature equal to 2.716×10^{-29} cm^{-1}/(molecule cm^{-2}) [63]. In Fig. 8(a) we show a single spectrum (blue diamonds) and the average of 984 spectra (black dots) obtained at a pressure of 26.7 kPa (200 Torr). The lower panels give fit residuals for the VP, SDVP, and GP fits to the averaged spectrum in which we have incorporated one etalon (denoted by green circles) in the analysis. Comparison of the single and averaged spectra indicates that the averaging technique yields a more than fifteenfold improvement in the

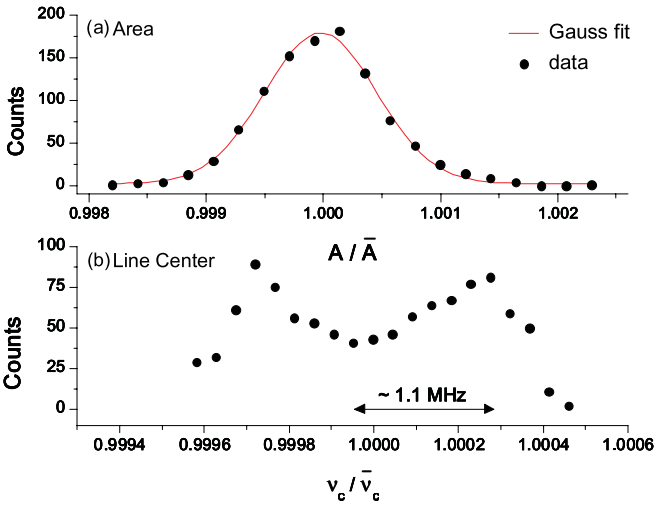

FIG. 7. (Color online) Histograms of measured line area (a) (with Gaussian fit) and line center (b) parameters for the R7 Q8 O_2 transition. Fluctuations of the line center (1.1 MHz) correspond to instability of the spectrum frequency axis. See text for details.

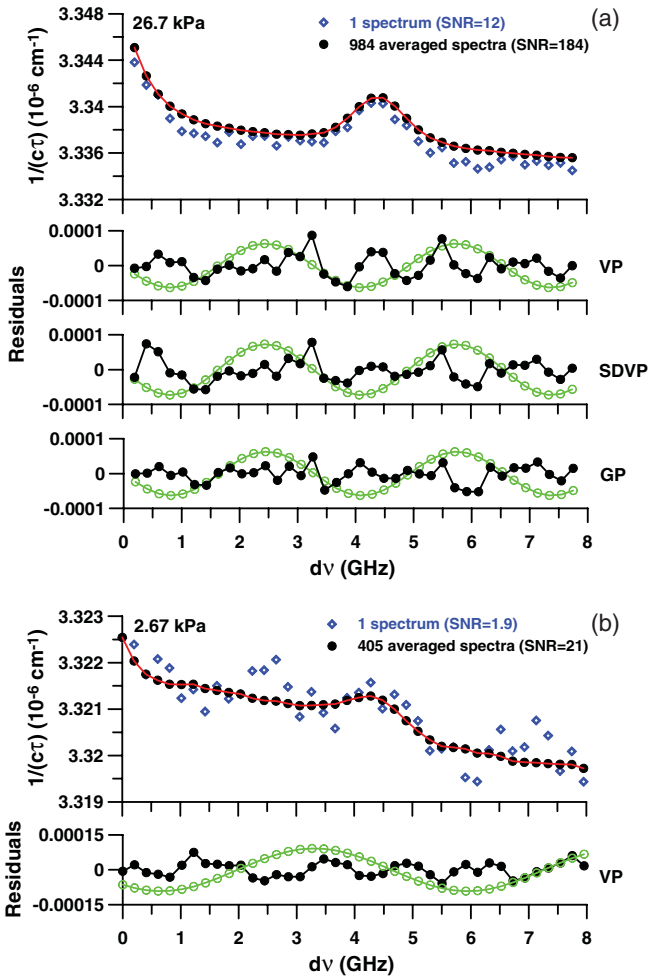

FIG. 8. (Color online) The spectrum of the R41 R41 O_2 line measured at pressures 26.7 kPa (a) and 2.67 kPa (b), respectively. In panel (a) single and averaged spectra ($N = 984$) as well as residuals from VP, SDVP, and GP fits are presented. In panel (b) single and averaged ($N = 405$) spectra as well as residual from the VP fit are presented. Single and averaged spectra are marked by blue diamonds and black dots, respectively. The etalon incorporated in the line-shape analysis was marked by green circles.

spectrum SNR, thus enabling quantitative analysis of the line parameters for this transition. Modeling the measured R41 R41 spectrum also required that absorption by the R7 Q8 $^{16}O^{17}O$ *B*-band line, which is 15 times stronger than the former, be taken into account. In Fig. 9 we show a spectral survey capturing both transitions in which we have averaged 44 spectra. The frequency separation between these two lines (based on the fitted line centers) is 5.182(9) GHz. For the results presented in Fig. 8(a), the worst fits were obtained when the VP was fit to the measured spectra. In this case, the symmetric w-shape structure near the line center on VP can be seen in the fit residuals. The application of the SDVP to the R41 R41 line-shape analysis reduced the magnitude of this w-shape structure, but did not remove it completely. Finally, the best results were obtained from GP fits. The line-shape parameters and statistical uncertainties obtained for the R41 R41 $^{16}O_2$ and R7 Q8 $^{16}O^{17}O$ lines are given in Table I. We note that the observed difference in fit quality between the SDVP and GP

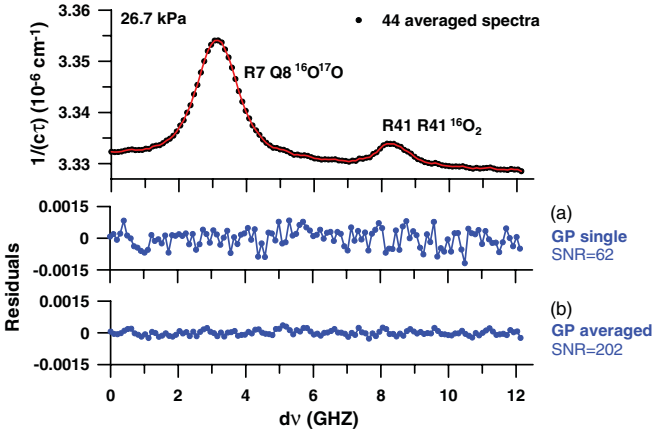

FIG. 9. (Color online) The spectrum of R41 R41 O_2 and R7 Q8 $^{16}O^{17}O$ lines at pressure 26.7 kPa. GP residuals for the single and 44 averaged spectra are presented below.

models is typical for the high-pressure range (see, for example, Ref. [40]). As was shown in Ref. [70], for low pressures the SDVP with the quadratic speed-dependence function and the GP give a similar fit quality. Finally, the difference in baselines between the single and averaged spectra shown in Fig. 8(a) is caused by systematic drift that occurred during these long-term measurements.

In order to determine the detection limit of our PDH-locked FS-CRDS spectrometer, we reduced the O_2 pressure to 2.67 kPa (20 Torr) and remeasured the R41 R41 *B*-band line. Under these conditions the interrogated line was barely detectable because of the extremely low SNR value of 1.9. A single spectrum of this line is given by the blue diamonds in Fig. 8(b). The minimum detectable absorption (MDA) calculated for this case is 3.7×10^{-10} cm^{-1} (VP fit) and is comparable to the noise amplitude obtained for the single spectrum shown in Fig. 5 (see the blue diamond graph). Averaging 405 spectra improved the SNR more than elevenfold compared to the single-spectrum SNR. Ideally, this should have resulted in a MDA value that is a factor of $\sqrt{405}$-fold lower than the single spectrum case, equal to 1.84×10^{-11} cm^{-1} (see the black dashed line for the R41 R41 $^{16}O_2$ transition in Fig. 5). This MDA value is consistent with our previous prediction in Ref. [60] for the present FS-CRDS system. However, because of drift in etalons and other systematic effects as described above, the reduction in noise produced by the spectrum averaging is slightly less than predicted, resulting in an actual MDA of about 2.4×10^{-11} cm^{-1} (see the red line for the R41 R41 $^{16}O_2$ transition in Fig. 5). For measurement of O_2, the MDA value that we achieved corresponds to a line intensity of the order of 1.3×10^{-30} cm^{-1}/(molecule cm^{-2}) measured at a SNR of 1 and a pressure 2.67 kPa.

V. CONCLUSION

In this study, we used the FS-CRDS technique to obtain exceptionally high signal-to-noise ratios and unprecedented spectral fidelity in line-shape measurements of the R7 Q8 $^{16}O_2$ *B*-band transition. The inherent stability of the FS-CRDS technique enabled long-term spectrum averaging, which reduced

statistical noise. We demonstrated a signal-to-noise ratio of 220 000 and line-shape distortions less than 1 part in 80 000 by averaging 1040 spectra obtained over a 33-hr time interval. The low level of line-shape distortion also required that slowly drifting etaloning effects be accounted for in the spectrum analysis. Fitting the measured line shape with an advanced profile such as the SDNGP enabled us to quantify the observed line asymmetry, which we assigned to speed dependence of the collisional shift. We emphasize that if the SNR is too low, this kind of asymmetry is difficult to observe in the pressure range of these measurements, particularly for self-colliding systems. For these reasons, this subtle line-shape effect was not observed in our previous measurements of the R7 Q8 $^{16}O_2$ line [64,65]. However, in the present study, application of the Pound-Drever-Hall laser-locking technique in our frequency-stabilized CRDS system and improvements in the measurement procedure (in particular the offset correction of the PDH-lock error signal [61]) yielded improved SNR and high spectral resolution. The only other absorption technique of which we are aware that yields a comparable dynamic range is the chirped-pulse Fourier-transform spectroscopy (CP-FTS). This technique has been demonstrated in the microwave (SNR $\sim$ 200 000) [90] and terahertz (SNR $\sim$ 100 000) [91] regions. However, CP-FTS requires samples with a permanent dipole moment and in the absence of double-resonance techniques cannot be used to directly probe most vibrational or electronic transitions. Furthermore, the wide dynamic range and low detection limit demonstrated here could motivate investigations of the symmetrization postulate. The work of Mazzotti *et al.* [45], which is based on high-sensitivity laser absorption spectroscopy to probe the $^{12}C^{16}O_2$ fundamental band at $\lambda = 4.22$ μm, is currently the most stringent test of this principle. Using the present FS-CRDS technique to probe this $^{12}C^{16}O_2$ band, we estimate that one could observe intensities as low as $\sim 1.8 \times 10^{-31}$ cm^{-1}/(molecule cm^{-2}), which would reduce the current upper bound on the symmetrization violation parameter (1.7×10^{-11}) by about two orders of magnitude. Recent developments in optical determination of the Boltzmann constant [92,93], which are based on the precise determination of the Doppler width, were enabled by progress in high-SNR laser absorption spectroscopy. High-SNR line-shape measurements such as those demonstrated here together with the advanced line-shape analyses [40] could lead to the determination of the Boltzmann constant with relative uncertainties at the 1 part in 100 000 or below.

We have also demonstrated a detection limit of 2.4×10^{-11} cm^{-1}, which is comparable to those obtained for other CRDS systems [30,31,83,94,95]. However, it should be noted that, in most cases, the previously reported low detection limits were due mainly to the application of low-loss cavity mirrors or to advantages of working in the near-infrared region where relatively low noise detectors are available for measuring ring-down decay signals (compare Refs. [94] and [30], see also Ref. [95]). Except for Ref. [31], the technique of spectrum averaging was treated as a secondary issue in these works. We estimate that the smallest measurable line intensity with our PDH-locked FS-CRDS incorporating spectrum averaging as described here is about 1.3×10^{-30}cm^{-1}/(molecule cm^{-2}).

ACKNOWLEDGMENTS

We would like to thank Dr. Alan S. Pine for valuable discussions and critical comments on this work. The research is part of the program of the National Laboratory FAMO in Toruń, Poland, and is supported by the Polish MNISW, Project No. N N202 1255 35. The research was partially supported by the Foundation for Polish Science TEAM Project co-financed by the EU European Regional Development Fund. A.C. is supported by the Polish NCN, Project No. N N202 2392 40. J.T.H. was supported in part by the National Institute of Standards and Technology (NIST) Greenhouse Gas and Climate Science Measurements Program.

[1] P. Duggan, P. M. Sinclair, R. Berman, A. D. May, and J. R. Drummond, J. Molec. Spectrosc. **186**, 90 (1997).
[2] A. S. Pine and R. Ciuryło, J. Molec. Spectrosc. **208**, 180 (2001).
[3] J. W. Brault, L. R. Brown, C. Chackerian Jr., R. Freedman, A. Predoi-Cross, and A. S. Pine, J. Molec. Spectrosc. **222**, 220 (2003).
[4] F. Rohart *et al.*, J. Molec. Spectrosc. **246**, 213 (2007).
[5] H. Tran, D. Bermejo, J. L. Domenech, P. Joubert, R. R. Gamache, and J.-M. Hartmann, J. Quant. Spectrosc. Radiat. Transfer **108**, 126 (2007).
[6] R. Wehr R. Ciuryło, A. Vitcu, F. Thibault, J. R. Drummond, and A. D. May, J. Molec. Spectrosc. **235**, 54 (2006).
[7] R. H. Dicke, Phys. Rev. **89**, 472 (1953).
[8] P. R. Berman, J. Quant. Spectrosc. Radiat. Transf. **12**, 1331 (1972).
[9] I. Gordon, L. S. Rothman, and G. C. Toon, J. Quant. Spectrosc. Radiat. Transfer **112**, 2310 (2011).
[10] C. E. Miller, L. R. Brown, R. A. Toth, D. Chris Benner, V. Malathy Devi, C. R. Phys. **6**, 876 (2005).
[11] A. S. Pine, J. Opt. Soc. Am. **64**, 1683 (1974).
[12] A. S. Pine, J. Opt. Soc. Am. **66**, 97 (1976).
[13] S. Nazemi, A. Javan, A. S. Pine, J. Chem. Phys. **78**, 4797 (1983).
[14] A. S. Pine, J. Chem. Phys. **101**, 3444 (1994).
[15] P. Duggan, P. M. Sinclair, A. D. May, and J. R. Drummond, Phys. Rev. A **51**, 218 (1995).
[16] A. S. Pine and V. N. Markov, J. Molec. Spectrosc. **228**, 121 (2004).
[17] D. Lisak, G. Rusciano, and A. Sasso, Phys. Rev. A **72**, 012503 (2005).
[18] H. Tran, D. Bermejo, J. L. Domenech, P. Joubert, R. R. Gamache, and J.-M. Hartmann, J. Quant. Spectrosc. Radiat. Transfer **108**, 126 (2007).
[19] R. Wehr, J. R. Drummond, and A. D. May, Appl. Opt. **46**, 978 (2007).
[20] R. S. Eng, A. R. Calawa, T. C. Harman, P. L. Kelley, and A. Javan, Appl. Phys. Lett. **21**, 303 (1972).
[21] P. L. Varghese and R. K. Hanson, Appl. Opt. **23**, 2376 (1984).

[22] A. Henry, D. Hurtmans, M. Margottin-Maclou, and A. Valentin, J. Quant. Spectrosc. Radiat. Transfer **56**, 647 (1996).

[23] B. Lance, G. Blanquet, J. Walrand, and J. P. Bouanich, J. Molac. Spectrosc. **185**, 262 (1997).

[24] F. Thibault, A. W. Mantz, C. Claveau, A. Henry, A. Valentin, and D. Hurtmans, J. Molec. Spectrosc. **246**, 118 (2007).

[25] D. Hurtmans, A. Henry, A. Valentin, and C. Boulet, J. Molec. Spectrosc. **254**, 126 (2009).

[26] J. W. Brault, L. R. Brown, C. Chackerian Jr., R. Freedman, A. Predoi-Cross, and A. S. Pine, J. Molec. Spectrosc. **222**, 220 (2003).

[27] A. Predoi-Cross, K. Hambrook, R. Keller, C. Povey, I. Schofield, D. Hurtmans, H. Over, and G. C. Mellau, J. Molec. Spectrosc. **248**, 85 (2008).

[28] V. M. Devi, D. C. Benner, C. E. Miller, and A. Predoi-Cross, J. Quant. Spectrosc. Radiat. Transfer **111**, 2355 (2010).

[29] J.-M. Hartmann, C. Boulet, and D. Robert, *Collisional Effects on Molecular Spectra: Laboratory Experiments and Model, Consequences for Applications* (Elsevier, Amsterdam, 2008).

[30] D. A. Long, M. Okumura, C. E. Miller, and J. T. Hodges, Appl. Phys. B **105**, 471 (2011).

[31] D. A. Long, D. K. Havey, M. Okumura, H. M. Pickett, C. E. Miller, and J. T. Hodges, Phys. Rev. A **80**, 042513 (2009).

[32] M. D. De Vizia, F. Rohart, A. Castrillo, E. Fasci, L. Moretti, and L. Gianfrani, Phys. Rev. A **83**, 052506 (2011).

[33] I. M. Mills, P. J. Mohr, T. J. Quinn, B. N. Taylor, and E. R. Williams, Metrologia **43**, 227 (2006).

[34] M. R. Moldover, J. P. M. Trusler, T. J. Edwards, J. B. Mehl, and R. S. Davis, Phys. Rev. Lett. **60**, 249 (1988).

[35] C. Daussy, M. Guinet, A. Amy-Klein, K. Djerroud, Y. Hermier, S. Briaudeau, C.J. Borde, and C. Chardonnet, Phys. Rev. Lett. **98**, 250801 (2007).

[36] G. Casa, A. Castrillo, G. Galzerano, R. Wehr, A. Merlone, D. Di Serafino, P. Laporta, and L. Gianfrani, Phys. Rev. Lett. **100**, 200801 (2008).

[37] K. M. T. Yamada, A. Onae, F.-L. Hong, H. Inaba, and T. Shimizu, C. R. Phys. **10**, 907 (2009).

[38] C. Lemarchand, K. Djerroud, B. Darquié, O. Lopez, A. Amy-Klein, C. Chardonnet, Ch. J. Bordé, S. Briaudeau, and C. Daussy, Int. J. Thermophys **31**, 1347 (2010).

[39] A. Merlone, F. Moro, A. Castrillo, and L. Gianfrani, Int. J. Thermophys. **31**, 1360 (2010).

[40] A. Cygan, D. Lisak, R. S. Trawiński, and R. Ciuryło, Phys. Rev. A **82**, 032515 (2010).

[41] C. J. Bordé, C. R. Phys. **10**, 866 (2009).

[42] M. D. De Vizia, L. Moretti, A. Castrillo, E. Fasci, and L. Gianfrani, Molec. Phys. **109**, 2291 (2011).

[43] M. de Angelis, G. Gagliardi, L. Gianfrani, and G. M. Tino, Phys. Rev. Lett. **76**, 2840 (1996).

[44] R. C. Hilborn and C. L. Yuca, Phys. Rev. Lett. **76**, 2844 (1996).

[45] D. Mazzotti, P. Cancio, G. Giusfredi, M. Inguscio, and P. De Natale, Phys. Rev. Lett. **86**, 1919 (2001).

[46] J. P. Uzan, Rev. Mod. Phys. **75**, 403 (2003).

[47] S. G. Karshenboim, Can. J. Phys. **83**, 767 (2005).

[48] M. Quack, J. Stohner, and M. Willeke, Annu. Rev. Phys. Chem. **59**, 741 (2008).

[49] D. C. Morton and G. W. F. Drake, Phys. Rev. A **83**, 042503 (2011).

[50] E. Kerstel and L. Gianfrani, Appl. Phys. B **92**, 439 (2008).

[51] D. A. Long, D. K. Havey, M. Okumura, C. E. Miller, J. T. Hodges, Phys. Rev. A **81**, 064502 (2010).

[52] A. Miani and J. Tennyson, Jour. Chem. Phys. **120**, 2732 (2004).

[53] A. Kuze and K. V. Chance, J. Geophys. Res. **99**, 14481 (1994).

[54] J. S. Daniel, S. Solomon, H. L. Miller, A. O. Langford, R. W. Portmann, and C. S. Eubank, J. Geophys. Res. **108**, 4515 (2003).

[55] D. A. Ortland, W. R. Skinner, P. B. Hays, M. D. Burrage, R. S. Lieberman, A. R. Marshall, and D. A. Gell, J. Geophys. Res. **101**, 10351 (1996).

[56] C. R. Nowlan, C. T. McElroy, and J. R. Drummond, J. Quant. Spectrosc. Radiat. Transf. **108**, 371 (2007).

[57] A. O'Keefe and D. A. G. Deacon, Rev. Sci. Instrum. **59**, 2544 (1988).

[58] J. T. Hodges, H. P. Layer, W. M. Miller, and G. E. Scace, Rev. Sci. Instrum. **75**, 849 (2004).

[59] J. T. Hodges and R. Ciuryło, Rev. Sci. Instrum. **76**, 023112 (2005).

[60] A. Cygan, D. Lisak, P. Masłowski, K. Bielska, S. Wójtewicz, J. Domysławska, H. Abe, J. T. Hodges, R. S. Trawiński, and R. Ciuryło, Rev. Sci. Instrum. **82**, 063107 (2011).

[61] A. Cygan, D. Lisak, S. Wójtewicz, J. Domysławska, R. S. Trawiński, and R. Ciuryło, Meas. Sci. Technol. **22**, 115303 (2011).

[62] R. W. P. Drever, J. L. Hall, F. V. Kowalski, J. Hough, G. M. Ford, A. J. Munley, and H. Ward, Appl. Phys. B **31**, 97 (1983).

[63] L. S. Rothman, I. E. Gordon, A. Barbe, D. C. Benner, P. F. Bernath, M. Birk, V. Boudon, L. R. Brown, A. Campargue, J.-P. Champion, K. Chance, L. H. Coudert, V. Dana, V. M. Devi, S. Fally, J.-M. Flaud, R. R. Gamache, A. Goldman, D. Jacquemart, I. Kleiner, N. Lacome, W. J. Lafferty, J.-Y. Mandin, S. T. Massie, S. N. Mikhailenko, C. E. Miller, N. Moazzen-Ahmadi, O. V. Naumenko, A. V. Nikitin, J. Orphal, V. I. Perevalov, A. Perrin, A. Predoi-Cross, C. P. Rinsland, M. Rotger, M. Šimečková, M. A. H. Smith, K. Sung, S. A. Tashkun, J. Tennyson, R. A. Toth, A. C. Vandaele, and J. V. Auwera, J. Quant. Spectrosc. Radiat. Transfer **110**, 533 (2009).

[64] D. Lisak, P. Masłowski, A. Cygan, K. Bielska, S. Wójtewicz, M. Piwiński, J. T. Hodges, R. S. Trawiński, and R. Ciuryło, Phys. Rev. A **81**, 042504 (2010).

[65] S. Wójtewicz, D. Lisak, A. Cygan, J. Domysławska, R. S. Trawiński, and R. Ciuryło, Phys. Rev. A **84**, 032511 (2011).

[66] L. Galatry, Phys. Rev. **122**, 1218 (1961).

[67] S. G. Rautian and I. I. Sobelman, Usp. Fiz. Nauk **90**, 209 (1966) [Sov. Phys. Usp. **9**, 701 (1967)].

[68] M. Nelkin and A. Ghatak, Phys. Rev. **135**, A4 (1964).

[69] B. Lance, G. Blanquet, J. Walrand, and J.-P. Bouanich, J. Mol. Spectrosc. **185**, 262 (1997).

[70] D. Priem, F. Rohart, J.-M. Colmont, G. Wlodarczak, and J.-P. Bouanich, J. Mol. Struct. **517**, 435 (2000).

[71] J. Ward, J. Cooper, and E. W. Smith, J. Quant. Spectrosc. Radiat. Transfer **14**, 555 (1974).

[72] R. Ciuryło, Phys. Rev. A **58**, 1029 (1998).

[73] I. Shannon, M. Harris, D. R. McHugh, and E. L. Lewis, J. Phys. B **19**, 1409 (1986).

[74] A. Bielski, R. Ciuryło, J. Domysławska, D. Lisak, R. S. Trawiński, and J. Szudy, Phys. Rev. A **62**, 032511 (2000).

[75] R. S. Trawiński, A. Bielski, and D. Lisak, Acta Phys. Pol. A **99**, 243 (2001).

[76] A. Urbanowicz, A. Bielski, D. Lisak, R. Ciuryło, and R. S. Trawiński, Eur. Phys. J. D **56**, 17 (2010).
[77] A. Urbanowicz, A. Bielski, D. Lisak, R. Ciuryło, and R. S. Trawiński, Eur. Phys. J. D **61**, 1 (2011).
[78] D. Lisak, G. Rusciano, and A. Sasso, J. Mol. Spectrosc. **227**, 162 (2004).
[79] D. Lisak, G. Rusciano, and A. Sasso, Phys. Rev. A **72**, 012503 (2005).
[80] D. Lisak, J. T. Hodges, and R. Ciuryło, Phys. Rev. A **73**, 012507 (2006).
[81] D. Lisak, D. K. Havey, and J. T. Hodges, Phys. Rev. A **79**, 052507 (2009).
[82] D. A. Long, K. Bielska, D. Lisak, D. K. Havey, M. Okumura, C. E. Miller, and J. T. Hodges, J. Chem. Phys. **135**, 064308 (2011).
[83] S. Kassi, D. Romanini, A. Camparague, and B. Bussery-Honvault, Chem. Phys. Lett. **409**, 281 (2005).
[84] L. Demeio, S. Green, and L. Monchick, J. Chem. Phys. **102**, 9160 (1995).
[85] J. Szudy and W. E. Baylis, J. Quant. Spectrosc. Radiat. Transfer **17**, 681 (1977).
[86] M. Baranger, Phys. Rev. **111**, 494 (1958).
[87] A. S. Pine, J. Quant. Spectrosc. Radiat. Transfer **62**, 397 (1999).
[88] D. W. Allan, Proc. IEEE **54**, 221 (1966).
[89] J. Domysławska, S. Wójtewicz, D. Lisak, A. Cygan, F. Ozimek, K. Stec, Cz. Radzewicz, R. Trawiński, R. Ciuryło, J. Chem. Phys. **136**, 024201 (2012).
[90] G. G. Brown, B. C. Dian, K. O. Douglass, S. M. Geyer, S. T. Shipman, and B. H. Pate, Rev. Sci. Instrum. **79**, 053103 (2008).
[91] E. Gerecht, K. O. Douglass, and D. F. Plusquellic, Opt. Expr. **19**, 8974 (2011).
[92] C. Lemarchand, M. Triki, B. Darquié, Ch. J. Bordé, C. Chardonnet, and C. Daussy, New J. Phys. **13**, 073028 (2011).
[93] A. Castrillo, M. D. DeVizia, L. Moretti, G. Galzerano, P. Laporta, A. Merlone, and L. Gianfrani, Phys. Rev. A **84**, 032510 (2011).
[94] D. K. Havey, D. A. Long, M. Okumura, C. E. Miller, and J. T. Hodges, Chem. Phys. Lett. **483**, 49 (2009).
[95] B. Gao, W. Jiang, A.-W. Liu, Y. Lu, C.-F. Cheng, G.-S. Cheng, and S.-M. Hu, Rev. Sci. Instrum. **81**, 043105 (2010).